Journal of
Ship&Ocean
Technology
©JUNE 2007

SOTECH Vol. 11, No. 2, pp. 10 ~ 25, 2007

Optimization of the Propeller Steady Performance Behind Wake Field

Wang-Soo Lee[1], Young-Dal Choi[2], Gun-Do Kim[3], Il-Sung Moon[3] and Chang-Sup Lee[1]

[1] Department of Naval Architecture and Ocean Engineering, Chungnam National Univ., Daejeon, Korea
[2] STX Shipbuilding Co., Ltd, Jinhae, Korea
[3] Maritime and Ocean Engineering Research Institute, KORDI, Daejeon, Korea;
Corresponding Author: csleepro@cnu.ac.kr

Abstract

With the sharp increase of the oil price, the issue of the energy saving requires even higher propulsive efficiency of the propellers. Traditionally the propellers have been designed with the criteria such as that of Lerbs optimum based on the lifting line theory and the empirical formulae of Lerbs and van Manen giving relations of the wake pitch with the wake non-uniformity. With the aid of the high speed computer, it is now possible to apply the time-consuming iterative approaches for the solution of the lifting surface problems. In this paper we formulate the variational problem to optimize the efficiency of the propeller operating in the given ship wake using the lifting surface method. The variational formulation relating the spanwise circulation distribution with the propulsive efficiency to be maximized is however non-linear in circulation distribution functions, thus the iterative method is applied to the quasi-linearized equations. The blade shape design also requires the iterative procedures, because the shape of the blade which is represented by the lifting surface is unknown a priori. The numerical code was validated with the DTNSRDC propeller 4119 which is well-known to be optimum in uniform inflow condition. In addition existing (well-designed) commercial propellers were selected and compared with the results of the open water tests and the self-propulsion tests.

Keywords: propeller, optimization, lifting surface theory, blade geometry, variational method

1 Introduction

The needs for optimum propellers in the circumferentially averaged wake fields are still increasing ever since the first appearance of the propellers as the propulsive device for marine vessels. With sharp increase of oil price, the procedure for the optimum propeller is desperately needed with the target of increasing 1 ~2 % of efficiency over the existing well-designed propeller.

Major sources of efficiency loss of marine propellers include the viscous drag associated with the skin friction on the blade surface and the kinetic energy related to the axial induced velocity and the rotational induced velocity shed in the propeller slipstream

by the action of the propeller while generating the thrust to propel the ship forward. Any method to improve the efficiency of the propeller is therefore closely associated with a method to reduce at least one of the sources of efficiency losses. One of the most favorite is to recover the rotational energy shed downstream from the blade by applying complex/compound configuration such as the pre/post-swirl vane, the contra-rotating propellers, etc. It is also possible to improve the efficiency by reducing the viscous drag through reduction of the expanded area while satisfying the same cavitation criteria. In principle, all the geometric parameters can be varied arbitrarily at the same time to find the optimum shape that produces the maximum efficiency obtainable. We will however select in this paper only two independent geometric quantities such as the pitch and camber distributions among many others, to make the problems as simple and cost-effective as possible, with the hope to correlate and to validate the optimization method with the experimental results.

One of the earliest criteria for the optimum efficiency of lightly-loaded propellers, due to Lerbs(1952), states that the ratio of the pitch of the undisturbed oncoming flow to the hydrodynamic pitch is a function of the local axial inflow velocity. This relation which is valid under the lifting-line approximation has been widely used for the initial guess of the circulation for the lifting-surface design procedures. These days the lifting-surface design is now the standard procedure, and therefore the initial input circulation to the lifting-surface code may better be replaced by the lifting-surface-generated optimum circulation distributions. Recently various propulsor optimization methods have been reported for the determination of the blade shape and the skews, where the optimization theories are applied with the aid of the lifting-surface programs. A typical lifting-surface code that may be of frequent use around the world is that of Kerwin and Lee(1978) for the analysis of both the steady and the unsteady performances of the propellers. The discrete vortex method(DVM), one of the well-established numerical lifting-surface theories, has been developed and improved at M.I.T., ever since the pioneering work of Kerwin(1961) on propellers, and thus it is not surprising to observe that Kerwin(1995) and Coney(1992) at M.I.T. developed a variational method based on the discrete vortex method for design optimization of the stand-alone propellers as well as the propulsors of complex/combined configuration. Olsen(2001) in Denmark developed a DVM procedure applying the same variational method as Coney to maximize the propulsive performance of the propellers, and could apply the optimization technique to develop the Kappel propellers(Andersen et al 2005). The Kappel propellers, raked sharply to the pressure side near the blade tip, indicate that the nonlinear effect of the loading may play an important role in optimization. Note however that most of the present day lifting surface design programs takes as input the circulation distribution obtained by the lifting-line approximation except Coney and Olsen who developed the lifting-surface optimization procedures. With the increase of power and speed of recent vessels, the loading on the blades are now reaching the critical points, and hence the Lerbs condition may be no longer a best approximation to the optimum condition for the moderately-/heavily-loaded propellers.

In the present paper, more accurate and consistent approach to get the optimum circulation distribution based on the lifting-surface approximation is developed, which will produce a propeller geometry with improved efficiency. The influence of the effective wake distribution on the propeller performance is not negligible, but it is a well-known practice that many propeller designers carry out their optimal design to achieve the maximum propeller open-water efficiency in the analysis of the self-propulsion test. In the present study, the optimization will be performed considering the effective velocity profiles,

and will be compared with the propellers optimized at the open-water condition. The variational method will be applied to the discrete vortex method code, as is done by Coney, to generate a set of simultaneous equations as a function of unknown discrete vortices. The propellers, optimized considering the condition behind the ship, will be evaluated through the self-propulsion tests in the towing tank.

2 Formulation of optimization problem

The ultimate goal of the propeller optimization is to maximize the quasi-propulsive efficiency, η_D. The present study however limits its scope to the problem of maximizing the time-mean propeller efficiency in the radially-varying but circumferentially-averaged effective velocity field. Our objective will be to find the optimum circulation giving the minimum torque, Q, subject to the condition of the prescribed thrust, T_{given}, at a given advance coefficient, J_A.

Introducing the Lagrange multiplier, λ, we may define a new object function, H, as:

$$H = Q - \lambda G \tag{1}$$

subject to the constraint, G, requiring the thrust, T, to meet the given thrust, T_{given}, as:

$$G = T - T_{given} = 0 \tag{2}$$

The distributed loading on the blades can in principle be represented by a system of continuous vortices, placed on the mean camber surface of the blades and their trailing wake sheets. These continuous vortices are then discretized into $N \times M$ vortex lattice on the blades, with N and M representing the number of spanwise discrete vortices in the chordwise and spanwise directions, respectively, and M streamwise strips extending to infinite downstream. Reference should be made to the numerical lifting-surface procedure of Kerwin and Lee(1978) for the rational discretization and subsequent numerical treatment of all the induced velocity computations. The vortex lattice can be replaced by a set of horseshoe vortices, which may be formed by a spanwise vortex segment of strength, Γ_{nm}, and trailing vortices starting from both ends of the spanwise vortex segment following the chordwise direction on the blades and the streamwise direction in the trailing wake region. The subscripts, n, m, to the horseshoe are introduced to distinguish the chordwise and the spanwise indices, respectively. The circulation on the m-th chordwise strip is then computed by adding the strength of the spanwise vortices on the m-th strip as:

$$\Gamma_m^T = \sum_{n=0}^{N-1} \Gamma_{n,m}, \quad \text{for } m = 0, \ldots, M-1 \tag{3}$$

We will here introduce the shape function S to generate a prescribed loading variation in the chordwise direction for a unit circulation on the strip. The strength of the n-th spanwise vortex element may then be expressed as:

$$\Gamma_{nm} = S_n \Gamma_m^T \text{ and } \sum_{n=0}^{N-1} S_n = 1 \tag{4}$$

A representative shape function S_n for a well-known NACA a=0.8 meanline takes the following form:

$$\begin{aligned} S_n &= 2\delta s/(1.0+a), \quad s_n \le 0.8 \\ S_n &= \delta s/(1.0-s_n)f, \quad s_n > 0.8 \end{aligned} \tag{5}$$

where $s_n = (n+0.25)\delta s$ denotes the fractional coordinate along the chord of the n-th discrete vortex, $\delta s = 1.0/N$ the chord of N equally-divided elements and $f = 2.0/((1.0+a)(1.0-a))$ is a constant.

Noticing that the spanwise vortex strength, Γ_{nm}, can be expressed by a known shape function S_n and a total circulation, Γ_m^T, by (4), we may expect that the forces on the blades can be expressed in terms of M discrete circulation distributions.

Applying the variational principle, we may take derivative of the object function, H, with respect to the a-th circulation, Γ_a^T, for a =0,...,M − 1:

$$\frac{\partial H}{\partial \Gamma_a^T} = \frac{\partial Q}{\partial \Gamma_a^T} - \lambda \frac{\partial G}{\partial \Gamma_a^T} = 0 \tag{6}$$

We also take derivative with respect to the Lagrange multiplier which will recover the constraint equation as:

$$\frac{\partial H}{\partial \lambda} = G = 0 \tag{7}$$

We now apply the Kutta-Joukowski theorem into the spanwise vortices to get the total force and torque on the blade:

$$\vec{F} = \sum_{nm} \rho \vec{V}_{nm} \times \vec{\delta}_{nm} \Gamma_{nm} \tag{8}$$

$$\vec{Q} = \sum_{nm} (\vec{r}_{nm} \times \vec{F}_{nm}) \tag{9}$$

where $\vec{V}_{nm}$ is the total velocity on the force point on the spanwise vortex element, $\vec{\delta}_{nm}$ the vortex segment vector, $\vec{F}_{nm}$ the Kutta-Joukowski force acting on the n,m-th vortex element and $\vec{r}_{nm}$ the force point position vector on the vortex segment. The thrust and torque are then computed as the axial component of (8) and (9) as:

$$T = -\vec{F} \cdot \hat{i} \text{ and } Q = \vec{Q} \cdot \hat{i} \tag{10}$$

where $\hat{i}$ is the unit vector in axial direction, taken positive pointing downstream.

If we expand the expression for the total velocity on the n,m-th force point in (8),

recalling (4), we may rewrite the force on the n,m-th element as:

$$\vec{F}_{nm} = \rho\left\{\vec{U}_{nm} + \sum_{j=0}^{M-1}\left(\sum_{i=0}^{N-1}\vec{V}^{*}_{nm,ij}S_i\right)\Gamma^T_j\right\} \times \vec{\delta}_{nm}S_n\Gamma^T_m \tag{11}$$

Where $\vec{U}_{nm}$ is the inflow velocity into the force point, $\vec{V}^{*}_{nm,ij}$ the induced velocity on the n,m-th force point due to the i,j-th horseshoe vortex of unit strength.

In order to evaluate (6), substituting the thrust and torque with (10), we need expression taking derivative of Q and G functions with respect to Γ^T_a as:

$$\begin{aligned}\frac{\partial Q}{\partial \Gamma^T_a} &= \rho\sum_n\left[\vec{r}_{na}\times\left\{\vec{U}_{na}\times\vec{\delta}_{na}S_n\right\}\right]\cdot\hat{i} \\ &+\rho\sum_{nm}[\{\vec{r}_{na}\times\{(\sum_i\vec{V}^{*}_{na,im}S_i)\times\vec{\delta}_{na}S_n\}\}\cdot\hat{i} \\ &+\{\vec{r}_{nm}\times(\sum_i\vec{V}^{*}_{nm,ia}S_i)\times\vec{\delta}_{nm}S_n\}\cdot\hat{i}]\Gamma^T_m\end{aligned} \tag{12}$$

$$\begin{aligned}\frac{\partial G}{\partial \Gamma^T_a} &= -\rho\sum_n\left[\vec{U}_{na}\times\vec{\delta}_{na}\cdot\hat{i}S_n\right] \\ &-\rho\sum_{nm}[\{(\sum_i\vec{V}^{*}_{na,im}S_i)\times\vec{\delta}_{na}\cdot\hat{i}S_n\} \\ &+\{(\sum_i\vec{V}^{*}_{nm,ia}S_i)\times\vec{\delta}_{nm}\cdot\hat{i}S_n\}]\Gamma^T_m\end{aligned} \tag{13}$$

The constraint equation (7) may be rearranged as:

$$\begin{aligned}&\rho\sum_{nm}[\{\vec{U}_{nm}\times\vec{\delta}_{nm}\cdot\hat{i}S_n\} \\ &+\{\sum_j(\sum_i\vec{V}^{*}_{nm,ij}S_i)\Gamma^T_j\times\vec{\delta}_{nm}\cdot\hat{i}S_n\}]\Gamma^T_m \\ &=-T_{given}\end{aligned} \tag{14}$$

For a =0,..., M−1, the equation (6) can be rearranged, recalling (12) and (13), into:

$$\begin{aligned}&\sum_m A_{am}\Gamma^T_m + A_{aM}\lambda \\ &=-\rho\sum_n\left[\vec{r}_{na}\times\left\{\vec{U}_{na}\times\vec{\delta}_{na}S_n\right\}\right]\cdot\hat{i} \\ &\equiv RHS_a\end{aligned} \tag{15}$$

The equation (14) may be rearranged into the same form as above:

$$\sum_m A_{Mm}\Gamma_m^T = T_{given} \equiv RHS_M \tag{16}$$

Combining the equations (15) for a =0,..., M−1 and the equation (16), we may derive an (M +1)×(M+1) simultaneous equations of the following form for the M unknown discrete circulation Γ_m^T and λ:

$$\begin{bmatrix} A_{0,0} & A_{0,1} & A_{0,2} & \cdots & A_{0,M-1} & A_{0,M} \\ A_{1,0} & A_{1,1} & & & A_{1,M-1} & A_{1,M} \\ A_{2,0} & & & & & A_{2,M} \\ \vdots & & & & & \vdots \\ A_{M-1,0} & & & & A_{M-1,M-1} & A_{M-1,M} \\ A_{M,0} & A_{M,1} & A_{M,2} & \cdots & A_{M,M-1} & 0 \end{bmatrix} \times \begin{bmatrix} \Gamma_0^T \\ \Gamma_1^T \\ \vdots \\ \Gamma_{M-1}^T \\ \lambda \end{bmatrix} = \begin{bmatrix} RHS_0 \\ RHS_1 \\ \vdots \\ RHS_{M-1} \\ -T_{given} \end{bmatrix} \tag{17}$$

We should notice here the simultaneous equations (17) is non-linear in Γ_m^T due to quadratic terms, and hence may need to linearize the simultaneous equations for efficient numerical computations. We know that the second term in (13), which is the induced velocity due to all the vortex system, is smaller than the first term representing the incoming flow. Similarly the second term in the bracket containing Γ_j^T in (14) is also smaller than the first term. We may update these small correction effects by replacing Γ_m^T by the previous solution in the iterative solution. The coefficient matrix A in (17) however has to be updated at each iteration step. Due to the smallness of the perturbation terms causing the non-linear effect, the speed of iteration is very fast, as will be shown later.

3 Blade shape design

Once the strength of the vortex lattice is known, it is possible to get the total velocity anywhere in the fluid domain including on the camber surface where the normal boundary condition is to be satisfied. As mentioned before, we will allow the variation of pitch and camber surface only among many other geometrical variables. Because we are using the discrete vortex method, we have to assume a surface, called the trial surface, where we distribute the vortex lattice. This trial surface is aligned with the total velocity computed through iterations. When converged, the pitch distribution and the camber surface shape are determined. We will employ the surface design procedure of Kim(1995) to form the three-dimensional surface geometry. The convergence speed to get the pitch and camber distribution is also very fast, requiring only a few iterations. Figure 1 shows schematically the optimization, shape design and analysis loop.

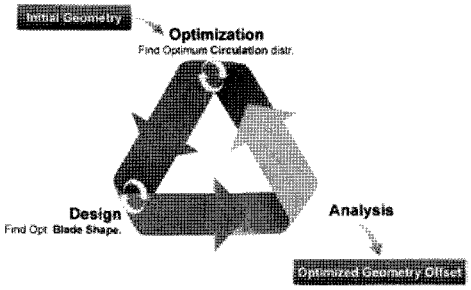

Figure 1: Diagram showing the optimization shape design and analysis loop

4 Fairing

The problem to look for the shape is more fragile than the analysis problem. Once a bad geometry is produced, the induced velocity calculation is accordingly affected by the bad geometry, and this in turn produces worse geometry. It gets worse as the iteration continues. It is very hard to include a restoring force without affecting the optimization procedure. This is especially true in the blade tip region. At present we do not include any artificial damping or restriction to the optimization code. Instead, we use in-house fairing tool, which enables us to control the geometry output from the code so that we can expect better geometrical characteristics from the designer's and manufacturer's points of view. Figure 2 shows a typical window that contains all the geometric information and buttons to perform the analysis, design and optimization procedures. Using this fairing tool, we may modify the output from the optimization code using the mouse or by keyboard inputs. Figures 3 and 4 show the typical pitch and camber distributions, respectively. Each figure contains the line of the parent design, that of the output from the optimization code and the manually modified line (with open dots). The manual work is performed by pulling the points with the mouse and we check the curvature along the curve as we do with the plastic battens in old drawing rooms

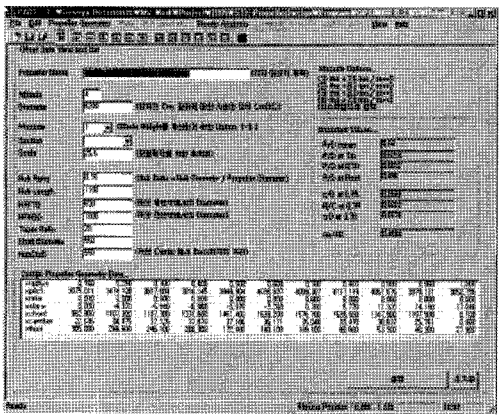

Figure 2: Typical window showing the geometric information

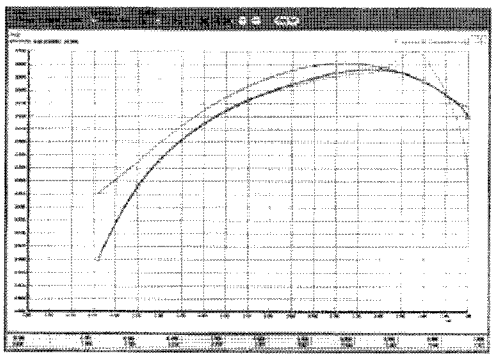

Figure 3: Typical pitch fairing process

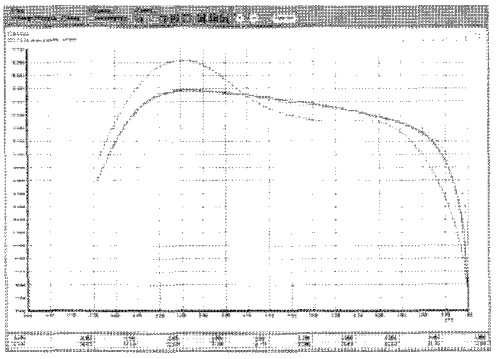

Figure 4: Typical camber fairing process

5 Validation of optimization code

For the validation of the propeller optimization code just developed, we selected two propellers. The first is DTNSRDC Propeller 4119(Jessup 1989), which is known to be optimum in uniform inflow condition. We will show how the new code produced geometry is close to the original constant pitch propeller. We then selected a modern bulk carrier, as seen in Table 1 for which we designed a new propeller optimized with the new program developed and carried out the propeller open-water tests and self-propulsion tests. The results of the new propellers are compared with the performance of the parent propellers.

Table 1: Ship Characteristic

Ship Type	Design Speed(knots)
Bulk Carrier	14.5

6 DTNSRDC propeller 4119

This propeller of three-blades has simple geometry; that is, the skew and the rake are all zero, and the pitch is (almost) constant over the radii. The expanded area ratio is 0.6 and the design advance coefficient J_A= 0.833. To make a fair comparison with the classical optimum condition, the Betz condition, both the optimization and the analysis codes used the non-deformed linear wake model, that is, the trailing wake has constant pitch and follows the pure helical surface.

Convergence tests: The convergence of the circulation distribution is plotted for Propeller 4119 in Figure 5, where, for circulation updates in (13) and (14), twenty(20) iterations are shown sufficient. Note in this figure the initial circulation obtained with all the nonlinear terms set equal to zero is far from the final circulation, but the convergence speed is rather high.

Comparative study: Figure 6 through 8 compares the circulation distribution, the pitch distribution and the camber distribution for Propeller 4119 and the optimized propellers. The circulation distribution in Figure 6 is seen very close, but the optimized circulation shows a shift of circulation peak toward the tip. It is observed throughout all the

comparative study that the optimized designs tend to have more loading (circulation) in the outer radii than in the inner radii. It is not clear at this point why the optimum circulation of Propeller 4119 is different from what is obtained by the new code. The computed thrust, torque and the efficiency for Propeller 4119 and the optimized propeller are practically identical to several significant digits. The difference in pitch distribution is most noticeable in the tip and hub regions. From Figures 7 and 8 we observe that the new code produces less angle of attack loadings in the hub and tip region, but these are compensated by the increased camber loadings. Since the chord-length in the tip region is relatively small, the difference in the tip region is considered not that significant.

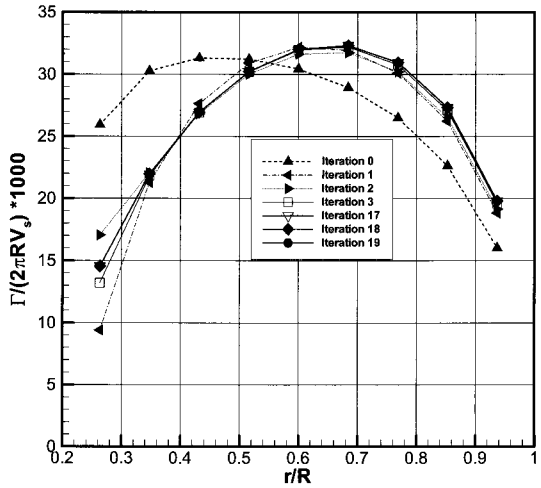

Figure 5: Convergence history of circulations through iterations for Propeller 4119

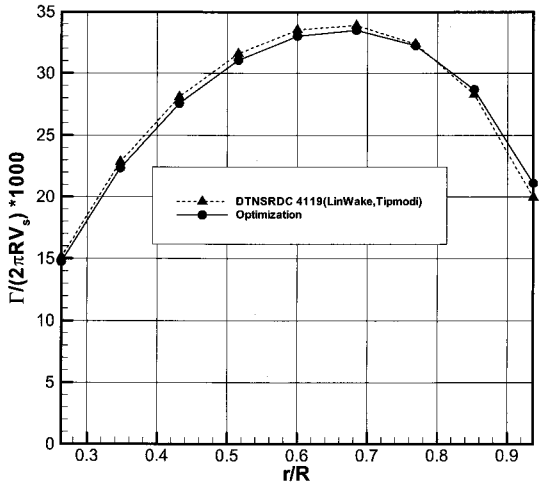

Figure 6: Comparison of the circulations for Propeller 4119

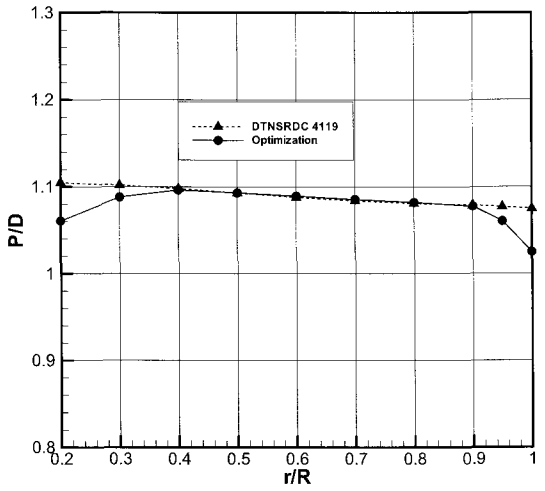

Figure 7: Comparison of the pitch distribution for Propeller 4119

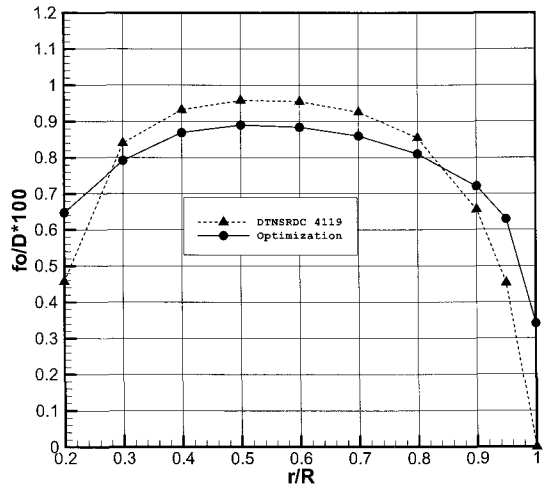

Figure 8: Comparison of the camber distribution for Propeller 4119

7 Bulk carrier propeller

The numerical experiment with DTNSRDC Propeller 4119 confirmed the validity of the present optimization scheme, and hence we proceeded to apply the same optimization technique to the existing vessel. We selected a modern medium-size bulk carrier, whose wake profile is shown in Figure 9. The effective wake profiles for the vessel is estimated from the radially-varying circumferentially-averaged nominal wake by applying the theoretical prediction method of Lee et al.(1991).

Usually the definition of the open-water propeller efficiency, η_o, is defined with the advance coefficient, J_A, the thrust coefficient, K_T, and the torque coefficient, K_Q, as:

$$\eta_o = \frac{J_A}{2\pi}\frac{K_T}{K_Q} \tag{18}$$

The efficiency in behind condition, or in the circumferentially-averaged wake, η_{CAW}, has to be defined slightly differently as:

$$\eta_{CAW} = \frac{Thrust\ power}{Input\ power} \tag{19}$$

The equations (18) and (19) are similar but the thrust power in (19) is considering the wake non-uniformity whereas the formula (18) can not consider the effect of the non-uniformity of the wake. For uniform wake, the equation (19) degenerates to (18).

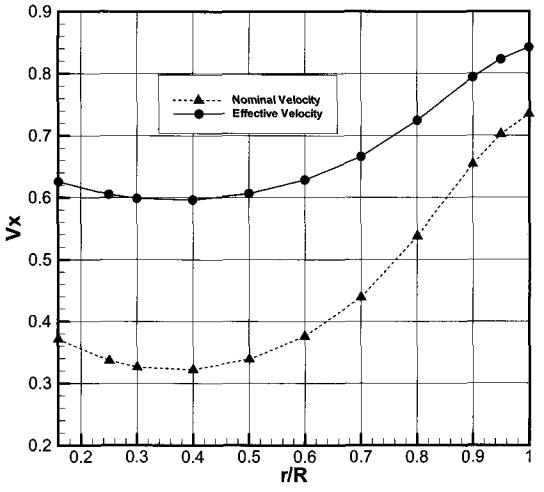

Figure 9: Comparison of the nominal and effective wake

The circulation distributions for the parent, the code-produced, and the faired propeller are all shown in Figure 10. The circulation distributions are very close to each other. But the optimization code produced pitch and camber distributions are clearly different from the parent ones. The pitch of the un-faired propeller shows a hump near r/R =0.9 with sharp decrease towards the tip. This kind of behavior is typical of the present optimization scheme.

It is not clear at this moment whether this is caused by the diverging nature of the geometry iteration scheme or is caused by the real non-linear physics of the flow in the tip region where the tip vortices are modeled to separate from the tip, as is demonstrated by Kerwin and Lee(1978), and the trailing wake is contracting sharply at/near the tip in Greeley and Kerwin's(1982) wake model.

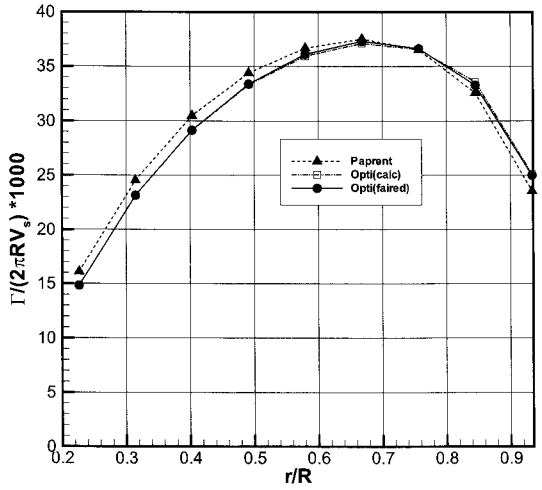

Figure 10: comparison of circulations of the parent, initial output and faired output

Due to the limit of resources to verify experimentally, we decided to fair out the pitch distribution in the tip region as in Figure 11. We also slightly modify the camber to have zero camber at the tip as in Figure 12. The representative parameters of the final output geometry are summarized in Table 2, and the three-dimensional view of the propeller is shown in Figure 13.

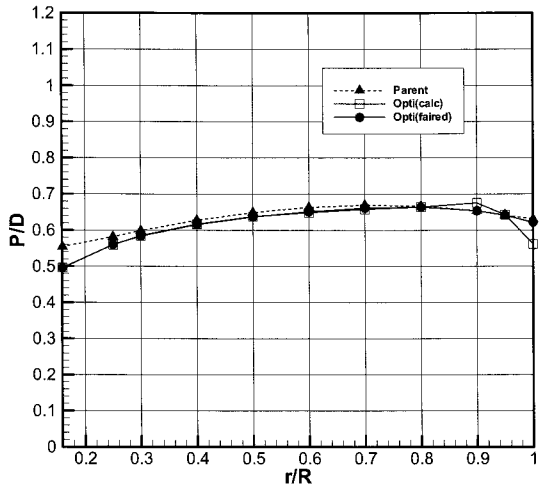

Figure 11: Comparison of parent pitch, initial output and faired pitch distr.

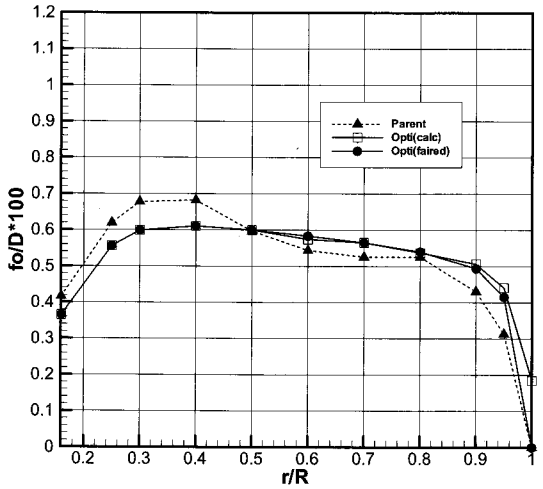

Figure 12: Comparison of parent camber, initial output camber and faired camber distr.

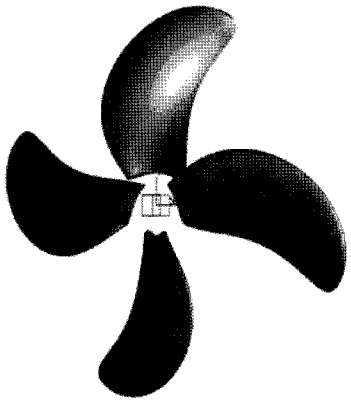

Figure 13: Three-dimensional view of Propeller

Table 2: Characteristics of parent(P) and optimized(O) propellers

.	Z	Ae/Ao	$(P/D)_m$	$(P/D)_7$	$(f_0/c)_7$
P	4	0.4594	0.6482	0.6697	0.0207
O	4	0.4594	0.6400	0.6612	0.0222

Z: number of blades
$(P/D)_m$: mean pitch ratio
$(P/D)_7$: pitch ratio at 0.7 r/R
$(f_0/c)_7$: (f_0/c) at 0.7 r/R

The DVM-predicted performance in the circumferentially averaged wake for propeller is summarized in Table 3. Comparing the efficiency for the parent and the optimized

propeller, we expect that the propeller-alone efficiency will improve about 0.6%. Unfortunately, the performance in CAW can not be experimentally verified.

Instead, we performed the self-propulsion tests with both propellers, and obtained the propulsive coefficient analyzed by ITTC 1978 prediction method and compared the coefficients at the same design speed as shown in Table 4. It is observed that the improvement in the quasi- propulsive efficiency, η_D, is only 0.5%.

Table 3: Propeller performance characteristic in CAW(circumferentially average wake)

	J	K_T	$10K_Q$	η_{CAW}
P	0.4100	0.1626	0.1809	0.5791
O	0.4100	0.1626	0.1804	0.5827

Table 4: Comparison of self-propulsion characteristics for parent and optimized propellers at the same design speed

	RR	η_o	η_R	η_H	η_D	RD
P	1.000	0.592	0.992	1.173	0.689	1.000
O	1.003	0.586	0.999	1.185	0.693	1.005

RR: Ratio of RPM(=RPM/parent RPM)
RD: Ratio of quasi-propulsive efficiency
(=η_D/parent η_D)

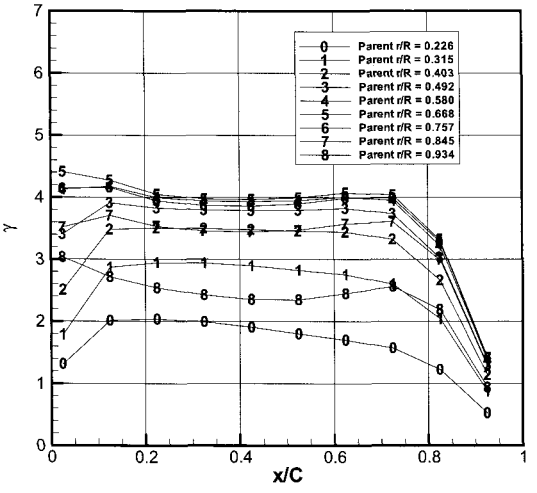

Figure 14: Chordwise loading distribution at various radii for parent propeller

It may be considered that the improvement is very small, even falling within the range of experimental errors, but through a careful exercises with a existing vessel, the improvement although not dramatic is present and can be achieved and verified by experiments.

To give some idea how the chordwise loading distributions are affected by the optimization program, we show Figures 14 and 15. We observe in both figures that the

chordwise vorticity distribution pattern follows the behavior of typical NACA a =0.8 meanline loading shape.

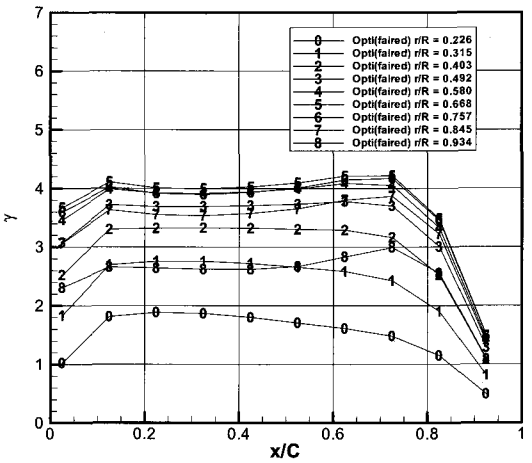

Figure 15: Chordwise loading distribution at various radii for optimized propeller

8 Conclusions

The optimization procedure based on the variational method is formulated to get the optimum circulation distribution using the numerical lifting-surface theory. The discrete circulation functions in the radial direction, serves as independent variables, are determined by solving the non-linear simultaneous equations obtained by variational formulations.

The numerical procedure, dealing with the non-linear terms through iteration, is found fast, efficient and robust. Comparative study with the well-known DTNSRDC Propeller 4119 shows that the new numerical code is reliable and produces a consistent result with the known optimum design.

Sample design optimization for an existing bulk carrier was performed, and the propeller model was manufactured and tested for the open-water and self-propulsion performances in the towing tank.

The gain in the quasi-propulsive efficiency is not significant, but is shown present and can be achieved and verified by experiments.

Considering the sharp oil price increase, the fractional percentage improvement in the efficiency is already not negligible.

The optimization code based on the discrete vortex method runs on the personal computer, is fast and easy to use. Even the beginners in propeller design practice can produce the same quality or even better propellers than the experienced engineers.

Acknowledgements

The authors would like to thank the STX Shipbuilding Co, Jinhae, Korea, for the financial support for the research and development program on propeller optimizations. The authors also thank Dr. Suak-Ho Van and Dr Hae-Sung Ahn of Maritime and Ocean Engineering

Research Institute (MOERI) for their cooperations for the analysis of the model experiments in the towing tank.

References

Andersen, P., J. Friesch, J. J. Kappel, L. Lundegaard and G. Patience. 2005. Development of a marine propeller with nonplanar lifting surfaces. Marine Technology, **42, 3,** 144-158.

Coney, W. B. 1992. Optimum circulation distributions for a class of marine propulsors. Journal of ship research, **36, 3,** 210-222.

Greeley, D. S. and J. E. Kerwin. 1982. Numerical Methods for Propeller Design and Analysis in Steady Flow. 8 Trans. of SNAME, **90,** 415-453.

Jessup, S. D. 1989. An experimental investigation of viscous aspects of propeller blade flow. Ph.D. Thesis, The Catholic Univ. of America.

Kerwin, J. E. 1961. The solution of propeller lifting surface problems by vortex lattice methods. Department of ocean engineering, MIT.

Kerwin, J. E. 1995. Hydrofoils and propellers. Department of ocean engineering, MIT.

Kerwin, J. E. and C. S. Lee. 1978. Prediction of steady and unsteady marine propeller performance by numerical lifting surface theory. Trans. of SNAME, **86,** 218-258.

Kim, J. H., S. K. Kim and C. S. Lee. 1995. Design of propeller blade shape by vortex distribution method. Proc. of 6-th International symposium on practical design of ships and mobile units, 17-22, **1,** 207-218.

Lee, C. S., Y. G. Kim and J. W. Ahn. 1991. Interaction between a propeller and the stern shear flow. Korea-Japan joint workshop on hydrodynamics in ship design, 16-29.

Lerbs, H. W. 1952. Moderately loaded propellers with a finite number of blades and an arbitrary distribution of circulation. Trans. of SNAME, **60,** 73-123.

Olsen, A. S. 2001. Optimisation of propellers using the vortex-lattice method. Ph.D. Thesis, Technical Univ. of Denmark.